Noname manuscript No.
(will be inserted by the editor)

Retinex by Higher Order Total Variation L^1 Decomposition

Jingwei Liang · Xiaoqun Zhang

Received: date / Accepted: date

Abstract In this paper we propose a reflectance and illumination decomposition model for Retinex via the high order total variation and L^1 decomposition. Based on the observation that illumination varies smoother than reflectance, we propose a convex variational model which can effectively decompose the gradient field of the observed image into salient edges and relatively smoother illumination field through the first and second order total variation regularization. The proposed model can be efficiently solved by a primal–dual splitting method. Numerical experiments on both grayscale and color images show the strength of the proposed model for applications to Retinex illusions, medical image bias field removal and color image shadow correction.

Keywords Retinex · Image decomposition · High-order total variation · Shadow correction

1 Introduction

In the past decades, the study of Retinex problem has inspired a wide range of applications and discussions [14,3,21]. The Retinex theory is originally proposed by Land and McCann [14] as a model of color perception of human visual system (HVS). The idea of Retinex theory is that HVS can ascertain reflectance of a field in which both illumination and reflectance are unknown. Our vision tends to see the same color of a given scene regardless of different illumination conditions. In other words, it ensures that the color of objects remains relatively constant under varying illumination. Figure 1[1] is the well-known Adelson's checkerboard shadow illusion. Visually, region A of Figure 1 (a) seems darker than region B , while digitally these two regions are of exactly the same intensity I. This phenomena is caused by different illumination conditions. The perceived intensity of the objects is the combination of reflectance and illumination. Taking into account the surroundings of the object (shadow of the cylinder, periodic pattern of the checkerboard), HVS can discount the illumination and perceive the reflectance automatically.

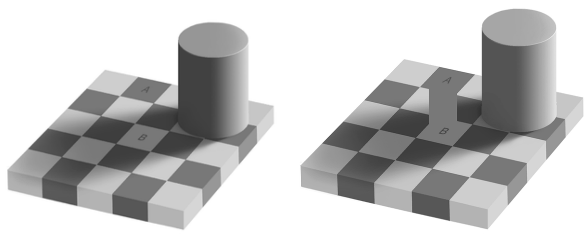

(a) original image (b) illusion free

Fig. 1: Checkerboard shadow illusion. (a) original checkerboard image, (b) illustration of illusion free image.

The primary goal of Retinex is to decompose a given image I into two components, the reflectance R and the

Jingwei Liang
GREYC, CNRS UMR 6072, ENSICAEN, Uni. de Caen. E-mail: jingwei.liang@ensicaen.fr

Xiaoqun Zhang
Department of Mathematics, MOE-LSC, and Institute of Natural Sciences, Shanghai Jiao Tong University. E-mail: xqzhang@sjtu.edu.cn

[1] http://web.mit.edu/persci/people/adelson/checkershadow_illusion.html

illumination L such that

$$I(x) = R(x) \times L(x), \tag{1}$$

for $x \in \Omega$ where $\Omega \subset \mathbb{R}^2$ is the domain of the image. To simplify the model, we can take a logarithm on (1) assuming that both R and L are positive and get

$$i(x) = r(x) + l(x). \tag{2}$$

Most of decomposition methods are based on the above additive model. The first Retinex algorithm proposed in [14] is based on path following, and further studied in [20,3]. Later on, the idea of path following is formulated into variational and PDE based models. In [21], Morel et al. show that if the light paths are assumed to be symmetric random walks, then Retinex solution satisfies a discrete Poisson equation and can be efficiently solved by using only two FFTs. Under variational framework, the followed total variation (TV) model proposed in [19] aims to extract piecewise constant reflectance r with data term in gradient field

$$\hat{r} = \arg\min_r \int_\Omega \Big(t|\nabla r| + \frac{1}{2}|\nabla r - \nabla i|^2\Big)\mathrm{d}x, \tag{3}$$

where t is a given positive weight parameter. This model is further modified in [18] to a simple L^1-based model

$$\hat{r} = \arg\min_r \int_\Omega |\nabla r - \delta_t(\nabla i)|\mathrm{d}x, \tag{4}$$

where $\delta_t(\nabla i)$ is a thresholded gradient field with respect to the parameter t. This model appears to be efficient on suppressing the lighting effect on the test images, however the loss of reflectance details and contrast can also be observed due to penalization on the magnitude of image gradient. Moreover a rigorous analysis of the proposed model is missing. Recently Zosso et al. [30] extended the TV based models to a unified non-local formulation.

Decomposition models by penalizing both r and l simultaneously are also very popular. For instance Kimmel et al. in [13] proposed the followed TV+H^1 decomposition model

$$\begin{aligned}\hat{r} = \arg\min_r \int_\Omega \big(|\nabla r| &+ \alpha(r-i)^2 \\ &+ \beta|\nabla(r-i)|^2\big)\mathrm{d}x,\end{aligned} \tag{5}$$

where the illumination $l = i - r$ is implicitly assumed to be smooth and penalized with H^1 norm. A similar model is further investigated by Ng and Wang in [22] with more constraints enforced. Specifically, the followed minimization problem over both r and l was proposed

$$\begin{aligned}\min_{r\le 0, l\ge i} \int_\Omega \Big(|\nabla r| &+ \frac{\alpha}{2}|\nabla l|^2 \\ &+ \frac{\beta}{2}(i-r-l)^2 + \frac{\mu}{2}l^2\Big)\mathrm{d}x.\end{aligned} \tag{6}$$

Here $l \ge i$ is based on the assumption that $0 < R \le 1$ and $r \le 0$.

In this paper, we also consider a decomposition approach to recover both r and l simultaneously. In particular, we focus on extracting the illumination field l using high order regularization. Our proposed model is closely related to recently developed high order total variation regularization. Therefore, in the following, we present some related models and notations.

1.1 High order total variation methods

It is well-known that the total variation regularization restoration [24] suffers the so-called staircase artifact. In order to suppress this effect, many higher order functionals have been studied since the pioneering infimal convolution model proposed in [5] on combining the first and second order total variation. The infimal convolution concerning two functionals ϕ and ψ is defined as

$$(\phi \triangle \psi)(u) = \inf_{u=v+w} \phi(v) + \psi(w).$$

The infimal convolution of the first and second order variations proposed in [5] takes the form

$$J_\beta(u) = \inf_{v+w=u} \int_\Omega |\nabla v|\mathrm{d}x + \beta\int_\Omega |\nabla^2 w|\mathrm{d}x, \tag{7}$$

where $\int_\Omega |\nabla^2 w|$ denotes the total variation of the Hessian of w for $w \in W^{2,1}(\Omega)$. Thus the image u can contain both piecewise constant and piecewise linear components. This formulation is restudied in [25,26] in the discrete setting for image restoration.

In a more general dual form, the infimal convolution of the first and the second order total variation is defined as

$$\begin{aligned}\mathrm{ICTV}_\beta(u) = \sup_{\substack{p\in I_1\\ q\in I_2}} \inf_w \int_\Omega \big((u-w)&\mathrm{div}(p) \\ &+ \beta w \mathrm{div}^2(q)\big)\mathrm{d}x,\end{aligned} \tag{8}$$

where $I_1 = \{p \in C_c^1(\Omega;\mathbb{R}^2), \|p\|_\infty \le 1\}$ and $I_2 = \{p \in C_c^2(\Omega;\mathbb{R}^{2\times 2}), \|p\|_\infty \le 1\}$. Note that if the symmetric Hessian is considered, we can also define $I_2 = \{p \in C_c^2\big(\Omega;\mathrm{Sym}^2(\mathbb{R}^2)\big), \|p\|_\infty \le 1\}$ where $\mathrm{Sym}^2(\mathbb{R}^2)$ denotes the space of symmetric matrices. Here, we abuse the notation of the infinity norm $\|\cdot\|_\infty$ in $C_c^1(\Omega;\mathbb{R}^2)$ and $C_c^2\big(\Omega;\mathrm{Sym}^2(\mathbb{R}^2)\big)$. A similar, yet different formulation, known as the total generalized variation (TGV), is proposed and rigorously studied in [4]. In particular, the second order TGV is defined as,

$$\begin{aligned}&\mathrm{TGV}_\beta^2(u)\\&=\sup_v\Big\{\int_\Omega u\mathrm{div}^2 v\mathrm{d}x \mid v\in \mathcal{C}_c^2(\Omega,\mathrm{Sym}^2(\mathbb{R}^2)),\\&\qquad\qquad \|v\|_\infty\le\beta,\ \|\mathrm{div}v\|_\infty\le 1\Big\}.\end{aligned}\tag{9}$$

In a simplified form, the alternative primal form of (9) is written as

$$\begin{aligned}\mathrm{TGV}_\beta^2(u)=\inf_{\boldsymbol{w}}\Big\{&\int_\Omega|\nabla u-\boldsymbol{w}|\mathrm{d}x\\&+\beta\int_\Omega|\nabla\boldsymbol{w}|\mathrm{d}x\Big\},\end{aligned}\tag{10}$$

where $\nabla\boldsymbol{w}\in\mathbb{R}^{2\times 2}$ is the (symmetrized) gradient of the deformation field $\boldsymbol{w}\in\mathbb{R}^2$. This formulation can be also viewed as replacing the decomposition $u=v+w$ in (7) with the decomposition of the gradient field $\nabla u=\nabla v+\boldsymbol{w}$. More discussions on the theoretical properties of the connections between the two functionals can be found in [4,1].

Another way of using high order TV is a direct combination, not the infimal convolution, of the first order and higher order regularization, such as [16,17,2,23]. For example [23] proposed a regularization model with direct combination of the first and second order regularization for image restoration

$$\begin{aligned}\min_u\Big\{&\frac{1}{2}\int_\Omega(Tu-u_0)^2\mathrm{d}x\\&+\alpha\int_\Omega|\nabla u|\mathrm{d}x+\beta\int_\Omega|D^2u|\mathrm{d}x\Big\},\end{aligned}$$

where T is a bounded linear operator and D is the gradient in distribute sense. This model has been studied in a more general and theoretical setting under the space of bounded Hessian. Finally, nonlinear high order regularization [8,27], combining with curvature line, such as Euler's elastic is also very popular, especially for image inpainting. In this paper, we focus more on the first and second order total variation.

1.2 Our contributions

The infimal convolution of the first and second total variation (in both ICTV and TGV) is designed to balance the first and high order singularities presented in images. By involving higher order derivatives, these functionals can capture higher order edges instead of only piecewise constant components. It has been shown that these methods can suppress staircase effects significantly.

From another point of view, the formulation (10) (and (7)) decomposes ∇u field into two parts, ℓ_1-norm of the residual $\nabla u-\boldsymbol{w}$ and TV semi-norm of $\boldsymbol{w}$. It has been known that TV+L^1 decomposition has interesting geometrical properties. As studied in [7,28], TV+L^1 decomposition model allows a scale dependent decomposition of geometry features, which is invariant to image contrast. In Retinex theory, as considered in previous path following based work, the illumination varies relatively slower, which can be considered as a relatively bigger scale in the gradient field. Furthermore, the nature of illumination often follows certain paths, thus piecewise linear approximation can model this behavior adequately.

This motivates us to consider a decomposition model to separate higher order piecewise smooth components from the edges of relatively smaller scale in the gradient field. In particular, we propose to decompose the image i into the illumination l and reflectance r, and set the regularization as

$$\begin{aligned}J(r)&=\int_\Omega|\nabla r|\mathrm{d}x,\\J_\beta(l)&=\beta\int_\Omega|\nabla^2 l|\mathrm{d}x.\end{aligned}\tag{11}$$

We call this proposed model as higher order total variation L^1 (HoTVL1) illumination and reflectance decomposition model. Close connections to the previous infimal convolution model (7) and (10) are shown, where we aim to extract the higher order singularities as the smoother illumination component. To the best of our knowledge, it is also the first time that the higher order infimal convolution model is used for the purpose of image decomposition. Furthermore, this model is different from the TV+H^1 decomposition model considered in [13,22], where the H^1 norm is penalized for the illumination. In the section of numerical results, we show that the proposed model can better separate the different scale of smoothness and singularities by the TV+L^1 decomposition in the gradient field. Moreover compared to the L^1-based model [18], the proposed method can preserve better the edges with small magnitude without smearing out the features in image with low intensities.

The paper is organized as following. In Section 2, we present the proposed model with constraints and discuss the connections to the previous higher order regularization models. Furthermore, the existence and uniqueness of the solution for the proposed method are rigorously discussed in an extended function space, i.e, the product space of the bounded variation and the bounded Hessian. In Section 3, a split inexact Uzawa based primal–dual splitting algorithm [29] is applied to solve the proposed model. Finally, we present numerical experiments on both synthetic gray scale images, visual illusion images, medical images with bias filed and real color image examples and compare the performance to some of the aforementioned existing variational based methods.

2 High Order TV+L^1 reflectance–illumination decomposition model

2.1 Proposed l model

Here, we present the first higher order TV+L^1 variational model for reflectance and illumination decomposition

$$\min_{r,l}\Big\{\mathcal{E}_{\alpha,\beta}(r,l)=\frac{1}{2}\int_\Omega(i-r-l)^2\mathrm{d}x + \alpha\Big(\int_\Omega|\nabla r|\mathrm{d}x+\beta\int_\Omega|\nabla^2 l|\mathrm{d}x\Big)\Big\}, \tag{12}$$

where l is the illumination and r is the reflectance, $\alpha>0,\beta>0$ are the regularization parameters.

Roughly speaking, we extract relatively smoother piecewise linear component as illumination l, and the texture part as r in gradient field for Retinex decomposition. Note that this model can be interpreted as the infimal convolution. The connections are shown as followed,

- If we let $u=r+l$, the model (12) is equivalent to minimize

$$\min_{u,l}\Big\{\frac{1}{2}\int_\Omega(u-i)^2\mathrm{d}x + \alpha\int_\Omega\big(|\nabla(u-l)|+\beta|\nabla^2 l|\big)\mathrm{d}x\Big\}, \tag{13}$$
$$\Longleftrightarrow \min_u\Big\{\frac{1}{2}\int_\Omega(u-i)^2\mathrm{d}x+\alpha\mathrm{ICTV}_\beta(u)\Big\}.$$

- If we further replace ∇l by $\boldsymbol{v}=\begin{bmatrix}v_1\\ v_2\end{bmatrix}$ in (12), we obtain the following model

$$\min_{u,\boldsymbol{v}}\Big\{\frac{1}{2}\int_\Omega(u-i)^2\mathrm{d}x + \alpha\int_\Omega\big(|\nabla u-\boldsymbol{v}|+\beta|\nabla\boldsymbol{v}|\big)\mathrm{d}x\Big\}, \tag{14}$$
$$\Longleftrightarrow \min_u\Big\{\frac{1}{2}\int_\Omega(u-i)^2\mathrm{d}x+\alpha\mathrm{TGV}^2_\beta(u)\Big\}.$$

Note that for both infimal convolution models, the illumination l is not explicitly given, while it can be extracted from the numerical scheme or solved through a Poisson equation $\nabla l=\boldsymbol{v}$ with boundary conditions.

Model (12) and the infimal convolution forms (13), (14) have some drawbacks if we are interested in the solutions of r and l. It is easy to see that any solution pair $(\hat r+c,\hat l-c)$ with c being a constant is still a solution, and this non-uniqueness may greatly affect the quality of the solution. Furthermore, to show the existence of the solution, the coercivity of the energy is also needed in the theoretical proof.

Therefore we consider an extended version of model (12), which imposes box constraints on both r and l components as

$$\min_{r\in\mathcal{B}_r,l\in\mathcal{B}_l}\Big\{\mathcal{E}_{\alpha,\beta,\tau}(r,l)=\frac{1}{2}\int_\Omega(i-r-l)^2\mathrm{d}x + \alpha\Big(\int_\Omega|\nabla r|\mathrm{d}x+\beta\int_\Omega|\nabla^2 l|\mathrm{d}x\Big) + \frac{\tau}{2}\int_\Omega l^2\mathrm{d}x\Big\}, \tag{15}$$

where τ is a small positive number to ensure the boundedness of l, $\mathcal{B}_r$ and $\mathcal{B}_l$ are the box constraints for r and l respectively. For instance, similar to the constraints considered by Ng and Wang [22], we consider $\mathcal{B}_r=]-\infty,0]$ and $\mathcal{B}_l=[i,+\infty[$ under the assumptions that the illumination R and I are normalized between $(0,1]$.

2.2 Existence and uniqueness of solution

The functional $\mathcal{E}_{\alpha,\beta,\tau}(r,l)$ in (15) is defined on $W^{1,1}\times W^{2,1}$. To establish the existence for such regularization, we usually need to discuss a larger Banach space for r and l. In particular, we consider r in the bounded variation space $\mathrm{BV}(\Omega)$ and l in $\mathrm{BH}(\Omega)$. Formally, we show the existence of the solution pair (r,l) of the following functional in the product space,

$$\min_{\substack{r\in\mathrm{BV}(\Omega)\\ l\in\mathrm{BH}(\Omega)}}\Big\{\mathcal{E}_{\alpha,\beta,\tau}(r,l)=\frac{1}{2}\|i-r-l\|^2 + \alpha\big(\|Dr\|_1+\beta\|D^2 l\|_1\big) + \frac{\tau}{2}\|l\|^2+\iota_{\mathcal{B}}(r,l)\Big\}, \tag{16}$$

where $\|\cdot\|$ denotes the norm in $L^2(\Omega)$, $\mathcal{B}$ denotes the box constraint set

$\mathcal{B}=\mathcal{B}_r\times\mathcal{B}_l,$

$\iota_{\mathcal{B}}(\cdot) = \iota_{\mathcal{B}_r}(r) + \iota_{\mathcal{B}_l}(l)$ is the corresponding indicator function, and $\|Dr\|_1$ and $\|D^2 l\|_1$ denotes the total variation of the first and second order derivatives in distribution sense, which will be defined in the following.

We first present some preliminaries for the bounded Hessian space proposed in [9] and in [2,23] in the context of image restoration. Let Ω be an open subset of $\mathbb{R}^n$ with Lipschitz boundary, recall that the Sobolev space $W^{1,1}(\Omega)$ is defined as

$$W^{1,1}(\Omega) = \left\{u \in L^1(\Omega) \,|\, \nabla u \in L^1(\Omega)\right\}.$$

The standard total variation semi-norm in distribution sense is defined as

$$\|Du\|_1 = \int_\Omega |Du|\mathrm{d}x = \sup_{\substack{p\in C_c^1(\Omega)^n\\ \|p\|_\infty \le 1}} \int_\Omega u \mathrm{div} p \mathrm{d}x, \tag{17}$$

where $\mathrm{div} p = \sum_{i=1}^n \frac{\partial p_i}{\partial x_i}(x)$. Let $\mathrm{BV}(\Omega)$ denote the space of bounded variation, i.e. $\mathrm{BV}(\Omega) = \left\{u \in L^1(\Omega) \,|\, \|Du\|_1 < \infty\right\}$.

Following Demengel [9] and [23], we consider the space of bounded Hessian functions, that we also call $\mathrm{BH}(\Omega)$ on extending the notion of total variation (17). Define

$$\begin{aligned}\|D^2 u\|_1 &= \int_\Omega |D^2 u|\mathrm{d}x \\ &= \sup_{\substack{\boldsymbol{\xi}\in C_c^2(\Omega;\mathbb{R}^{n\times n})\\ \|\boldsymbol{\xi}\|_\infty \le 1}} \int_\Omega \langle \nabla u, \mathrm{div}(\boldsymbol{\xi})\rangle \mathrm{d}x,\end{aligned} \tag{18}$$

where $\mathrm{div}(\boldsymbol{\xi}) = (\mathrm{div}\xi_1, \cdots, \mathrm{div}\xi_n)$ with

$$\forall i, \xi_i = \left\{\xi_i^{(1)}, \cdots, \xi_i^{(n)}\right\} \in \mathbb{R}^n,\ \mathrm{div}\xi_i = \sum_{k=1}^n \frac{\partial \xi_i^{(k)}}{\partial x_k},$$

and $\|\xi\|_\infty = \sup_{x\in\Omega} \sqrt{\sum_{i,j=1}^n |\xi_i^{(j)}(x)|^2}$. The space $\mathrm{BH}(\Omega)$ (also called as $\mathrm{BV}^2(\Omega)$ in [2]) consists of all functions $u \in W^{1,1}(\Omega)$ whose distributional Hessian is a finite Radon measure, i.e.

$$\mathrm{BH}(\Omega) = \left\{u \in W^{1,1}(\Omega) \,|\, \|D^2 u\|_1 < \infty\right\}.$$

It is immediate to see that $W^{2,1}(\Omega) \subset \mathrm{BH}(\Omega)$ and $\mathrm{BH}(\Omega)$ is a Banach space equipped with the norm $\|u\|_{\mathrm{BH}(\Omega)} = \|u\|_1 + \|\nabla u\|_1 + \|D^2 u\|_1$, where $\|\cdot\|_1$ denotes the L^1 norm in the corresponding space. In the following, we summarize some definitions and main properties in $\mathrm{BH}(\Omega)$, which can be found in [9,2,23]:

- (A weak* topology) Let $\{u_k\}_{k\in\mathbb{N}}$, u belong to $\mathrm{BH}(\Omega)$. The sequence $\{u_k\}$ converges to u weakly* in $\mathrm{BH}(\Omega)$ if

$$\begin{aligned}&\|u_k - u\|_1 \to 0,\ \ \|\nabla u_k - \nabla u\|_1 \to 0,\\ &\int_\Omega \langle \nabla u_k, \mathrm{div}(\boldsymbol{\xi})\rangle \mathrm{d}x \\ &\qquad \longrightarrow \int_\Omega \langle \nabla u,\ \mathrm{div}(\boldsymbol{\xi})\rangle \mathrm{d}x, \forall \boldsymbol{\xi} \in C_c^2(\Omega;\mathbb{R}^{n\times n}).\end{aligned} \tag{19}$$

- (Lower semi-continuity) The semi-norm $\|D^2 u\|_1$ is lower semi-continuous endowed with strong topology of $W^{1,1}(\Omega)$. More precisely, if $\|u_k - u\|_1 \to 0$ and $\|\nabla u_k - \nabla u\|_1 \to 0$, then

$$\|D^2 u\|_1 \le \liminf_{k\to\infty} \|D^2 u_k\|_1.$$

  In particular, for $\{u_k\}_{k\in\mathbb{N}} \in W^{1,1}(\Omega)$, if

$$\liminf_{k\to\infty} \|D^2 u_k\|_1 < \infty,$$

  then $u \in \mathrm{BH}(\Omega)$.

- (Compactness in $\mathrm{BH}(\Omega)$) Suppose that $\{u_k\}_{k\in\mathbb{N}}$ is bounded in $\mathrm{BH}(\Omega)$, then there exists a subsequence $\{u_{k_j}\}_{j\in\mathbb{N}}$ and $u \in \mathrm{BH}(\Omega)$ such that $\{u_{k_j}\}_{j\in\mathbb{N}}$ weakly* converges to u.

- (Embedding) If Ω has a Lipschitz boundary and it is connected, then it can be shown that there exists positive constants C_1, C_2 such that

$$\|\nabla u\|_1 \le C_1 \|D^2 u\|_1 + C_2 \|u\|_1, \tag{20}$$

  and $\mathrm{BH}(\Omega)$ is continuously embedded in $L^2(\Omega)$ when $n = 2$.

In the following, we use the above mentioned properties of $\mathrm{BH}(\Omega)$ together with similar ones of $\mathrm{BV}(\Omega)$ to establish the existence and the uniqueness of solution for the variational problem (16).

Theorem 1 *Suppose $i \in L^2(\Omega)$ and the parameters $\alpha, \beta, \tau > 0$, then the minimization problem (16)*

$$\min_{r,l} \mathcal{E}_{\alpha,\beta,\tau}(r, l)$$

has a unique solution $(r^*, l^*) \in \mathrm{BV}(\Omega) \times \mathrm{BH}(\Omega)$.

Proof Let $\{(r_k, l_k)\}_{k\in\mathbb{N}}$ be a minimizing sequence for (16). And let $M > 0$ be the upper bound for the minimizing sequence and

$$\|r_k + l_k - i\|^2 < M,\ \ \|l_k\|^2 < M, \tag{21}$$

$$\|Dr_k\|_1 < M,\ \ \|D^2 l_k\|_1 < M, \tag{22}$$

$$r_k \in \mathcal{B}_r,\ \ l_k \in \mathcal{B}_l, \tag{23}$$

for every $k \in \mathbb{N}$. Since $\{l_k\}_{k\in\mathbb{N}}$ is uniformly bounded in $L^2(\Omega)$, it is easy to see that $\{r_k\}_{k\in\mathbb{N}}$ is also uniformly bounded in $L^2(\Omega)$ combining the equations (21) and $i \in L^2(\Omega)$. Furthermore, by the boundedness of Ω, the sequence $\{r_k\}$ is bounded in $L^1(\Omega)$ and moreover bounded in $\mathrm{BV}(\Omega)$ since $\|Dr_k\|_1 < M$.

For $\{l_k\}$, we can similarly derive that $\{l_k\}$ is bounded in $L^1(\Omega)$. By virtue of the embedding inequality (20), we also have

$$\|\nabla l_k\|_1 < C_1\|D^2 l_k\|_1 + C_2\|l_k\|_1 < M',$$

where M' is a constant number for every $k \in \mathbb{N}$. Thus $\{l_k\}$ is uniformly bounded in $\mathrm{BH}(\Omega)$.

From the compact theorem in both BV and BH space, we obtain the existence of a subsequence (r_{k_j}, l_{k_j}) converges weakly* to (r^*, l^*) in $\mathrm{BV}(\Omega) \times \mathrm{BH}(\Omega)$. It is easy to see that the functional is proper since any constant function l and r has finite energy. Furthermore, the overall functional $\mathcal{E}_{\alpha,\beta,\tau}$ is convex and l.s.c under weak topology, the constraint sets $\mathcal{B}_r$ and $\mathcal{B}_l$ are closed, therefore we can derive that the minima can be attained at (r^*, l^*) by the theory of calculus of variation. It is also straightforward to see that the solution is unique since the functional is strongly convex with respect to (r, l).

3 Primal–dual splitting algorithm

In this section, we present the algorithm to solve the discretized model of (15). The problem has two unknowns r and l, and an alternating scheme will lead to separable and easy sub-problems on r and l. This method was also adopted in [22]. However, the alternating scheme does not guarantee the whole sequence convergence to the minimizer of the optimization problem. In this paper we are interested in solving r and l simultaneously, on preserving separable structures. Nowadays many techniques based on operator splitting can be applied to convex separable minimization, such as the split Bregman method [12], primal–dual splitting methods [10,6]. Here we adopt the split inexact Uzawa (SIU) method developed in [29], which yields a simple iteration scheme. More connections between different splitting algorithms can be found in [10], and the references therein.

In the following, we define some variables and notations to simplify the problem (15). Denote

$$x = \begin{bmatrix} r \\ l \end{bmatrix}, \quad A = \begin{bmatrix}\mathrm{Id}, & \mathrm{Id}\end{bmatrix}, \quad B = \begin{bmatrix}0, & \mathrm{Id}\end{bmatrix},$$

and the auxiliary ones

$$u = \nabla r, \quad v = \nabla^2 l,$$
$$y = \begin{bmatrix} u \\ v \end{bmatrix}, \quad \text{and} \quad L = \begin{bmatrix} \nabla, & 0 \\ 0, & \nabla^2 \end{bmatrix}.$$

Here we use the forward difference and Neumann boundary conditions for the discrete gradient and the symmetrized Hessian. In $\mathbb{R}^2$, for $u \in W^{1,1}(\Omega)$, define $D(\nabla u) = \frac{1}{2}(D + D^T)(\nabla u) = \begin{bmatrix} \xi_{11}, & \xi_{12} \\ \xi_{21}, & \xi_{22} \end{bmatrix}$ as the symmetrized Hessian

$$\begin{aligned} &\xi_{11} = \frac{\partial v_1}{\partial x_1}, \ \xi_{22} = \frac{\partial v_2}{\partial x_2}, \\ &\xi_{12} = \xi_{21} = \frac{1}{2}\Big(\frac{\partial v_1}{\partial x_2} + \frac{\partial v_2}{\partial x_1}\Big), \end{aligned} \tag{24}$$

for $\boldsymbol{v} = \begin{bmatrix} v_1 \\ v_2 \end{bmatrix} = \nabla u$ and the divergence can be defined accordingly.

We further define the following functionals:

$$H(x) = \frac{1}{2}\|i - Ax\|^2,$$
$$J(x, y) = \alpha\|y\|_{1,\beta} + \iota_{\mathcal{B}}(x) + \frac{\tau}{2}\|Bx\|^2.$$

where $\|y\|_{1,\beta} = \|u\|_1 + \beta\|v\|_1$. As a result, problem (15) can be formulated into the following form

$$\min_{x,y} H(x) + J(x, y) \ \text{ s.t. } \ Lx = y, \tag{25}$$

whose corresponding augmented Lagrangian formula is

$$\begin{aligned} \max_p \min_{x,y} \Big\{ &\mathcal{L}(p; x, y) = H(x) + J(x, y) \\ &+ \langle p, Lx - y\rangle + \frac{\nu}{2}\|Lx - y\|^2 \Big\}, \end{aligned} \tag{26}$$

where $p = \begin{bmatrix} p_r \\ p_l \end{bmatrix}$ is the Lagrangian multiplier.

The SIU method is an inexact alternating direction of multiplier method (ADMM) [11] applied to the above problem with an extra proximal term for the update of x^{k+1}, and the iterative scheme reads as

$$\begin{cases} x^{k+1} = \arg\min_x \mathcal{L}(p^k; x, y^k) + \frac{1}{2}\|x - x^k\|_{M_\nu}, \\ y^{k+1} = \arg\min_y \mathcal{L}(p^k; x^{k+1}, y), \\ p^{k+1} = p^k + \nu(Lx^{k+1} - y^{k+1}), \end{cases} \tag{27}$$

where M_ν is a positive definite matrix. To obtain an easy iterative scheme, we choose $M_\nu = \mathrm{Id} - \nu L^T L$, where $0 < \nu < 1/\|L^T L\|$ such that M_ν is positive definite.

In the following, we present a brief derivation for the update of x^{k+1} and y^{k+1}.

Update of x^{k+1} :

The update of x^{k+1} from (27), substituting M_ν with $\mathrm{Id} - \nu L^T L$, reads

$$\begin{aligned} x^{k+1} &= \arg\min_x \mathcal{L}(p^k; x, y^k) + \frac{1}{2}\|x - x^k\|^2_{M_\nu} \\ &= \arg\min_x \iota_{\mathcal{B}}(x) + \frac{1}{2}\|i - Ax\|^2 \\ &\quad + \frac{\tau}{2}\|Bx\|^2 + \frac{1}{2}\|x - w^k\|^2, \end{aligned} \tag{28}$$

where $w^k = x^k - L^T(\nu L x^k + p^k - \nu y^k) = \begin{bmatrix} w_r^k \\ w_l^k \end{bmatrix}$. The corresponding first order optimality condition of (28) is

$$\begin{aligned} 0 &\in N_{\mathcal{B}}(x) + A^T(Ax - i) + \tau B^T B x + (x - w^k) \\ &\in \begin{bmatrix} N_{\mathcal{B}_r}(r) \\ N_{\mathcal{B}_l}(l) \end{bmatrix} + \begin{bmatrix} r + l - i \\ r + l - i \end{bmatrix} + \tau \begin{bmatrix} 0 \\ l \end{bmatrix} + \begin{bmatrix} r - w_r^k \\ l - w_l^k \end{bmatrix}. \end{aligned}$$

Let $\tilde{w}_r = w_r^k + i, \tilde{w}_l = w_l^k + i$, and $\mathcal{P}_{\mathcal{C}}$ be the projection operator onto a convex set $\mathcal{C}$. In the following, we discuss the updating formula according to the different scenarios of the box constraints $\mathcal{B}$.

– If $\mathcal{B}_l = \mathbb{R}$, which implies that there is no constraint on l, we have the equations

$$\begin{cases} N_{\mathcal{B}_r}(r) + 2r + l = \tilde{w}_r, \\ \quad r + (\tau + 2)l = \tilde{w}_l. \end{cases}$$

By substituting the second equation in the first one, we obtain

$$N_{\mathcal{B}_r}(r) + \frac{2\tau + 3}{\tau + 2} r = \tilde{w}_r - \frac{\tilde{w}_l}{\tau + 2}$$

Thus the update formula for r^{k+1} and l^{k+1} read

$$\begin{cases} r^{k+1} = \mathcal{P}_{\mathcal{B}_r}\left(\dfrac{(\tau + 2)\tilde{w}_r - \tilde{w}_l}{2\tau + 3}\right), \\ l^{k+1} = \dfrac{\tilde{w}_l - r^{k+1}}{\tau + 2}. \end{cases}$$

– If $\mathcal{B}_r = \mathbb{R}$, similarly we get the equations

$$\begin{cases} \quad 2r + l = \tilde{w}_r, \\ 2N_{\mathcal{B}_l}(l) + (2\tau + 3)l = 2\tilde{w}_l - \tilde{w}_r. \end{cases}$$

And the update formula for r^{k+1} and l^{k+1} are

$$\begin{cases} l^{k+1} = \mathcal{P}_{\mathcal{B}_l}\left(\dfrac{2\tilde{w}_l - \tilde{w}_r}{2\tau + 3}\right), \\ r^{k+1} = \dfrac{\tilde{w}_r - l^{k+1}}{2}. \end{cases}$$

– If both $\mathcal{B}_r$ and $\mathcal{B}_l$ are not the whole space and this sub-problem is coupled on r and l, we apply an alternating projection method. The alternating projection scheme for this sub-problem reads

$$\begin{cases} r \leftarrow \mathcal{P}_{\mathcal{B}_r}\left(\dfrac{\tilde{w}_r - l}{2}\right), \\ l \leftarrow \mathcal{P}_{\mathcal{B}_l}\left(\dfrac{\tilde{w}_l - r}{2 + \tau}\right). \end{cases} \tag{29}$$

Note that in theory many iterations are needed for this step to get accurate r^{k+1}, l^{k+1}.

Update of y^{k+1} :

The update of y^{k+1} is straightforward. As $\|y\|_{1,\beta} = \|u\|_1 + \beta\|v\|_1$ is separable, we have

$$\begin{aligned} y^{k+1} &= \arg\min_y \mathcal{L}(p^k; x^{k+1}, y) \\ &= \arg\min_y \alpha\|y\|_{1,\beta} + \frac{\nu}{2}\|y - Lx^{k+1} - p^k/\nu\|^2 \\ &= \arg\min_{u,v} \alpha\|u\|_1 + \frac{\nu}{2}\|u - \nabla r^{k+1} - p_r^k/\nu\|^2 \\ &\quad + \alpha\beta\|v\|_1 + \frac{\nu}{2}\|v - \nabla^2 l^{k+1} - p_l^k/\nu\|^2, \end{aligned}$$

which leads to the following two simple threshold steps

$$\begin{cases} u^{k+1} = \mathcal{T}_{\alpha/\nu}(\nabla r^{k+1} + p_r^{k+1}/\tau), \\ v^{k+1} = \mathcal{T}_{\alpha\beta/\nu}(\nabla^2 l^{k+1} + p_l^{k+1}/\tau), \end{cases} \tag{30}$$

where $\mathcal{T}_\gamma(a) = \max(\|a\| - \gamma, 0)\frac{a}{\|a\|}$ is the isotropic soft-thresholding operator. Finally, the update for the dual variable p^{k+1} is straightforward.

To this end, combining (29), (30) and the update of p^{k+1} (27) we obtain the iteration scheme for solving the model (15).

4 Numerical Tests

To demonstrate the performance of our proposed method, in this section, we consider several image decomposition problems, including synthetic examples, Retinex illusion examples, medical image biased field removal and color image shadow correction. We compare our proposed method (15) (HoTVL1) to two recent variational methods (4) (MMO) and (6) (NW) proposed in [18] and [22] respectively.

Through the test, the recovered r of the MMO method and our proposed method are direct outputs from the model, so is for the NW model for the synthetic example and the Retinex problem. While for the bias field removal and color image shadow correction, the output r of the NW method is obtained via $i - l$, where l is the reconstructed illumination.

4.1 Synthetic images

We start with synthetic image examples with two different cases. As shown in Figure 2, the two piecewise constant images r present different geometry properties, so are the corresponding shadows l with piecewise smooth structures, and the simulated image is the sum of them $i = r + l$.

Decomposition results are shown in Figure 3 and 4. As we can observe, MMO and the proposed model produce better visual results than the NW method on these examples. Intuitively, NW method penalizes the ℓ_2-norm of the gradient of the shadow and it is not contrast invariant and the recovered illumination l contains more information of the edges of the reflectance. On the contrast, only very weak signal of r are contained in the recovered illumination l by MMO method and our proposed method. This will be further demonstrated in Retinex illusions and color image examples.

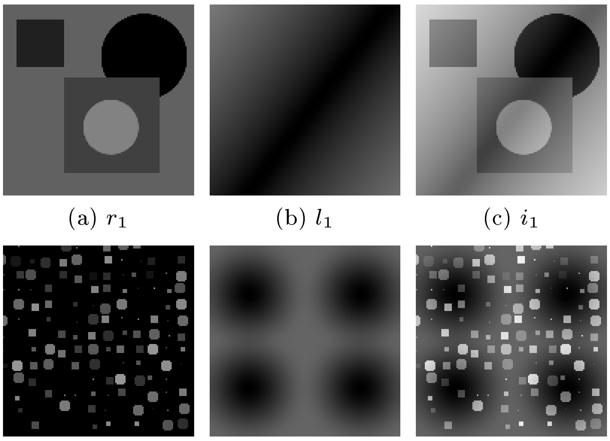

(a) r_1 (b) l_1 (c) i_1 (d) r_2 (e) l_2 (f) i_2

Fig. 2: Two synthetic images examples. (a) synthetic image r_1, (b) synthetic shadow l_1, (c) composed image $i_1 = r_1 + l_1$; (d) synthetic image r_2, (e) synthetic shadow l_2, (f) composed image $i_2 = r_2 + l_2$.

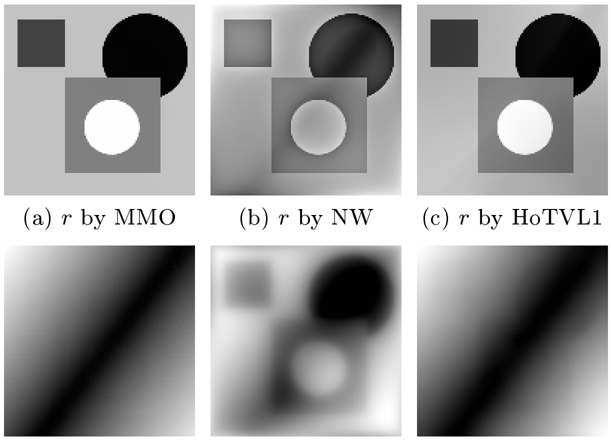

(a) r by MMO (b) r by NW (c) r by HoTVL1 (d) l by MMO (e) l by NW (f) l by HoTVL1

Fig. 3: Decomposition comparison of synthetic example 1. From top to bottom and from left to right: recovered reflectance r and illumination l by MMO, NW, and the proposed model.

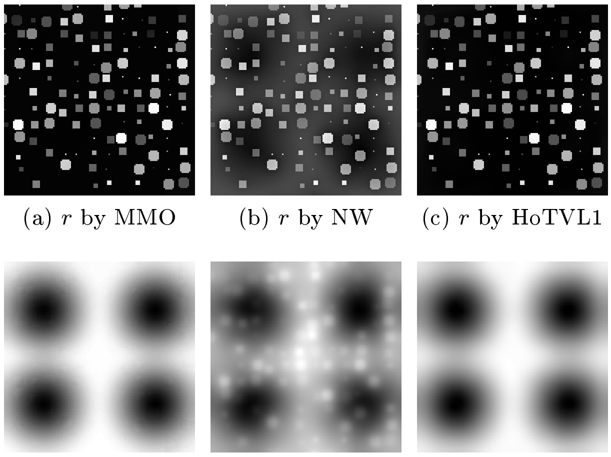

(a) r by MMO (b) r by NW (c) r by HoTVL1 (d) l by MMO (e) l by NW (f) l by HoTVL1

Fig. 4: Decomposition comparison of synthetic example 2. From top to bottom and from left to right: recovered reflectance r and illumination l by MMO, NW, and the proposed model.

4.2 Retinex illusion

The aforementioned checkerboard shadow image and the Logvinenko's cube shadow illusion image [15], as shown in Figure 5, are tested for Retinex illusion. For both images, though visually the region B is brighter than the region A, they are of the same intensity value, as marked in Figure 5.

Table 1 shows the comparison of the recovered gray values of the two regions A, B of the 3 methods. Our proposed method recovers the best contrast compared to the other two methods for both images.

Image		original	MMO	NW	HoTVL1
checker-board	A	120	80	90	85
	B	120	145	125	174
cube	A	140	26	85	10
	B	140	191	110	250

Table 1: Recovered gray value of the two regions A and B of the two images.

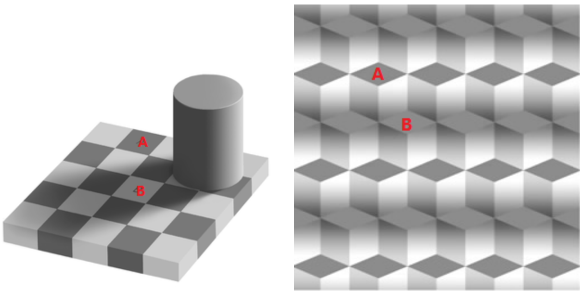

(a) checkerboard (b) cube

Fig. 5: Two test images for Retinex illusion. (a) Adelson's checkerboard shadow image, the gray value of the marked area is 120. (b) Logvinenko's cube shadow image, the gray value of the marked area is 140.

Figure 6 shows the visual comparison of the checkerboard image. Similar to the synthetic example, MMO and the proposed model obtain visually preferable outputs, however the recovered illumination in our proposed method contains less reflectance information compared to MMO. Also, the MMO method favors piecewise constant reflectance. Similar conclusions can be drawn from the comparison of the cube image, see Figure 7.

It can be noticed that the brightness of MMO method's result and ours is very different, especially in Figure 7. This is mainly due to the fact that for the MMO method, the gray value of the top left pixel is used to solved the Poisson equation, also the right column and bottom row of the output is brighter than the image domain because of the boundary condition.

In this test, $\beta = 10$ for both examples, and we set $\alpha = 4$ for the checkerboard image, and $\alpha = 10$ the cube image. The box constraints are $\mathcal{B}_r = [0, 255]$ and $\mathcal{B}_l = [-255, 0]$ for both images.

4.3 Medical image bias field correction

In medical imaging, obtained images may be corrupted by bias fields due to non-uniform illumination, for instance in parallel MRI imaging. The correction of the bias field is similar to Retinex problem that we need to remove the light effect caused by illumination. In the following, we adopt the setting discussed in [18]. Figure 8 shows the comparison of the methods, and all the methods can provide visual preferable results compared to the original ones, especially for the bottom part of the images.

For this example, we set $\alpha = 0.1$ and $\beta = 20$. The box constraints are $\mathcal{B}_r = [-20, 0]$ and $\mathcal{B}_l = [-20, 0]$ after taking the logarithm, and I is pre-scaled to $(0, 1]$.

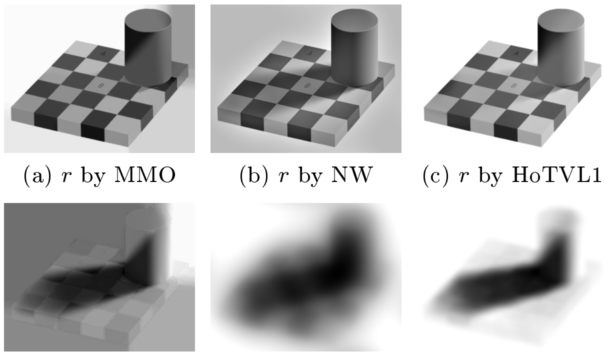

(a) r by MMO (b) r by NW (c) r by HoTVL1

(d) l by MMO (e) l by NW (f) l by HoTVL1

Fig. 6: Decomposition comparison of the checkerboard example. From top to bottom and from left to right: recovered reflectance r and illumination l by MMO, NW, and the proposed model.

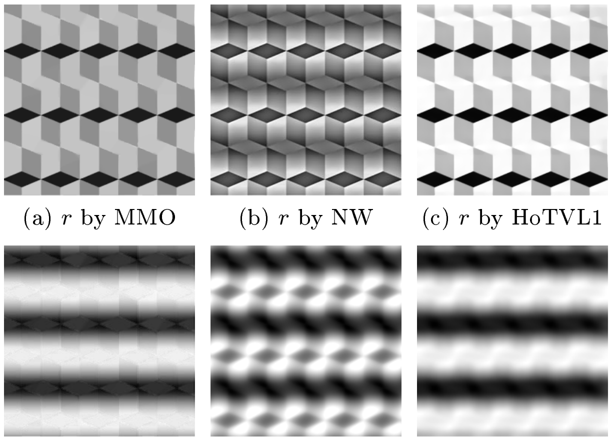

(a) r by MMO (b) r by NW (c) r by HoTVL1

(d) l by MMO (e) l by NW (f) l by HoTVL1

Fig. 7: Decomposition comparison of the cube example. From top to bottom and from left to right: recovered reflectance r and illumination l by MMO, NW, and the proposed model.

4.4 Color image shadow correction

The final illustrative example is on the correction of shadowed color image. For the two color images given in Figure 9(a) and 11(a), we choose the HSV color space and only process the V channel, on assuming that the shadow only affect on the brightness of the image, not the hue and saturation components. Figure 9 shows the comparison of the methods on the text image. Note that NW method also uses the γ-correction as post-processing, which may improve the white balance for under exposed image. We can see that the estimated shadow by our method is visually more accurate and the shadow effect can be partially removed in the recovered

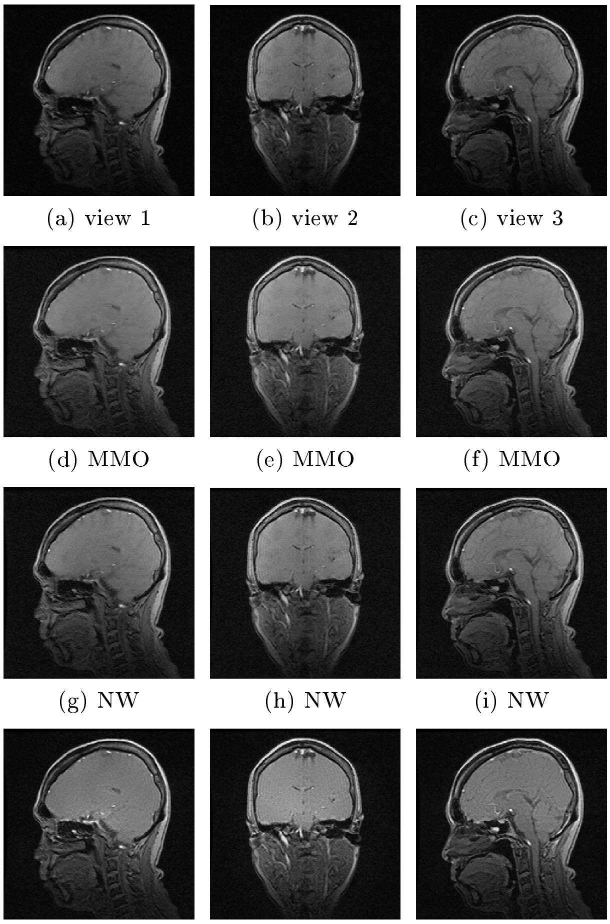

(a) view 1 (b) view 2 (c) view 3

(d) MMO (e) MMO (f) MMO

(g) NW (h) NW (i) NW

(j) HoTVL1 (k) HoTVL1 (l) HoTVL1

Fig. 8: MRI image bias field removal. (a), (d), (g), (j): image view 1 and the result of the 3 methods; (b), (e), (h), (k): image view 2 and the result of the 3 methods; (c), (f), (i), (l): image view 3 and the result of the 3 methods.

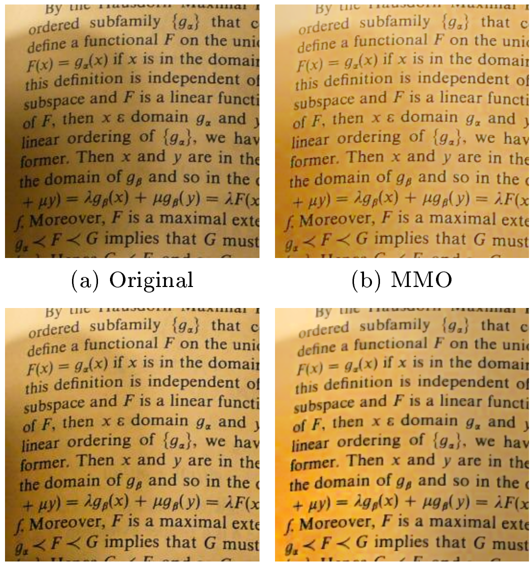

(a) Original (b) MMO

(c) NW (d) HoTVL1

Fig. 9: Comparison of recovered reflectance r on Text image.

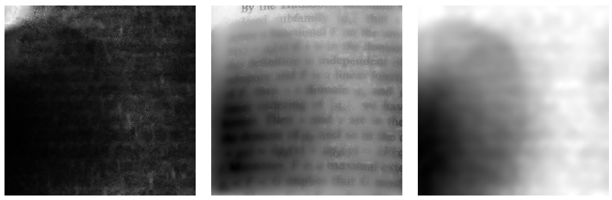

(a) MMO (b) NW (c) HoTVL1

Fig. 10: Comparison of recovered illumination l on Text image.

reflectance image. Similar observation can be obtained from Figure 11.

For this test, we set $\alpha = 1/12$ for text image and $1/10$ for the wall image, $\beta = 100$ is fixed. The box constraints are as same as the bias field correction's.

4.5 Computational time

To conclude this part, we present the time comparison of the 3 methods. Since we have box constraints for both r and l, inner iteration is needed for the update of x^{k+1}, and the number of iteration is set as 1 in all the tests. Among the methods, MMO method is the fastest due to its simplicity, NW method is the second, and our proposed method is more time consuming due to the two orders of regularization. For example in the synthetic example with image size 128×128, less than 1 second for the MMO method, around 1 second for the NW, while it take about 15 seconds for our method. However, we note that the computation time of our method can be improved by choosing a more efficient algorithm for solving the optimization algorithm.

5 Conclusions

In this paper, we have present a novel reflectance and illumination decomposition model based on high order total variation regularization. The so-called high order TV+L^1 decomposition is closely related to infimal convolution of first and second order regularization. The proposed model can nicely separate the relatively smoother piecewise linear component, which is modeled as the global illumination, from the relatively detailed reflectance edges. The numerical tests on in-

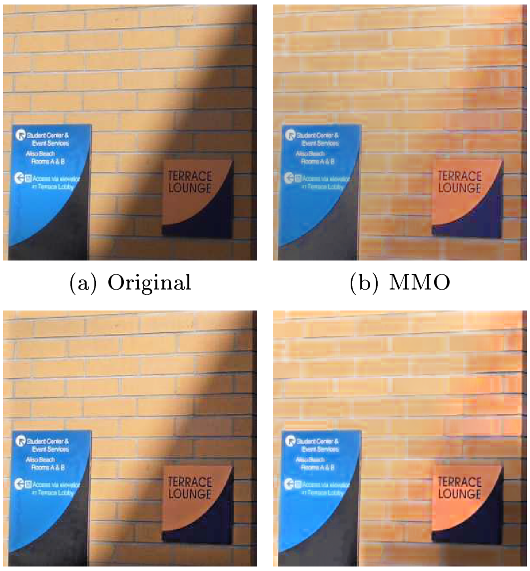

(a) Original (b) MMO

(c) NW (d) HoTVL1

Fig. 11: Comparison of recovered reflectance r on Wall image.

(a) MMO (b) NW (c) HoTVL1

Fig. 12: Comparison of recovered illumination l on Wall image.

homogeneous background removal and color correction have show that our proposed model extract a light field which is closer to human visual system and the image contrast in the restored reflectance with better preserved details, comparing to other decomposition model [22] and regularization in gradient methods [19].

Acknowledgements We would like to thank the authors of [19] and [22] for sharing their codes, and the reviewers of this manuscript for their helpful comments and suggestions. The work of X. Zhang was supported by NSFC11101277, NSFC91330102.

References

1. Benning, M., Brune, C., Burger, M., Müller, J.: Higher-order TV methods–enhancement via Bregman iteration. J. Sci. Comput. **54**(2-3), 269–310 (2013). DOI 10.1007/s10915-012-9650-3. URL http://dx.doi.org/10.1007/s10915-012-9650-3
2. Bergounioux, M., Piffet, L.: A second-order model for image denoising. Set-Valued and Variational Analysis **18**(3-4), 277–306 (2010). DOI 10.1007/s11228-010-0156-6. URL http://dx.doi.org/10.1007/s11228-010-0156-6
3. Bertalmío, M., Caselles, V., Provenzi, E.: Issues about retinex theory and contrast enhancement. International Journal of Computer Vision **83**(1), 101–119 (2009). DOI 10.1007/s11263-009-0221-5. URL http://dx.doi.org/10.1007/s11263-009-0221-5
4. Bredies, K., Kunisch, K., Pock, T.: Total generalized variation. SIAM Journal on Imaging Sciences **3**(3), 492–526 (2010). DOI 10.1137/090769521. URL http://epubs.siam.org/doi/abs/10.1137/090769521
5. Chambolle, A., Lions, P.L.: Image recovery via total variation minimization and related problems. Numerische Mathematik **76**(2), 167–188 (1997). DOI 10.1007/s002110050258. URL http://dx.doi.org/10.1007/s002110050258
6. Chambolle, A., Pock, T.: A first-order primal-dual algorithm for convex problems with applications to imaging. Journal of Mathematical Imaging and Vision **40**(1), 120–145 (2011). URL http://dx.doi.org/10.1007/s10851-010-0251-1
7. Chan, T.F., Esedoḡlu, S.: Aspects of total variation regularized l1 function approximation. SIAM Journal on Applied Mathematics **65**(5), pp. 1817–1837 (2005). URL http://www.jstor.org/stable/4096154
8. Chan, T.F., Kang, S.H., Kang, Shen, J.: Euler's elastica and curvature based inpaintings. SIAM J. Appl. Math **63**, 564–592 (2002). URL http://dx.doi.org/10.1137/S0036139901390088
9. Demengel, F.: Fonctions à hessien borné. Annales de l'institut Fourier **34**(2), 155–190 (1984). URL http://eudml.org/doc/74627
10. Esser, E., Zhang, X., Chan, T.F.: A general framework for a class of first order primal-dual algorithms for convex optimization in imaging science. SIAM J. Imaging Sci. **3**, 1015–1046 (2010). URL http://dx.doi.org/10.1007/s10915-010-9408-8
11. Gabay, D.: Applications of the method of multipliers to variational inequalities, *Augmented Lagrangian Methods: Applications to the Solution of Boundary-Value Problems*, vol. 15, chap. IX, pp. 299–331 (1983)
12. Goldstein, T., Osher, S.: The split Bregman method for l1-regularized problems. SIAM J. Img. Sci. **2**(2), 323–343 (2009). DOI 10.1137/080725891. URL http://dx.doi.org/10.1137/080725891
13. Kimmel, R., Elad, M., Shaked, D., Keshet, R., Sobel, I.: A variational framework for retinex. International Journal of computer vision **52**(1), 7–23 (2003). URL http://dx.doi.org/10.1023/A:1022314423998
14. LAND, E.H., McCANN, J.J.: Lightness and retinex theory. J. Opt. Soc. Am. **61**(1), 1–11 (1971). DOI 10.1364/JOSA.61.000001. URL http://www.opticsinfobase.org/abstract.cfm?URI=josa-61-1-1
15. Logvinenko, A.D.: Lightness induction revisited. PERCEPTION-LONDON- **28**, 803–816 (1999). URL http://dx.doi.org/10.1068/p2801
16. Lysaker, M., Lundervold, A., Tai, X.C.: Noise removal using fourth-order partial differential equation with applications to medical magnetic resonance images in space and time. Image Processing, IEEE Transactions on **12**(12), 1579–1590 (2003). URL http://dx.doi.org/10.1109/TIP.2003.819229
17. Lysaker, M., Tai, X.C.: Iterative image restoration combining total variation minimization and a second-order functional. International Journal of Computer Vision

66(1), 5–18 (2006). DOI 10.1007/s11263-005-3219-7. URL http://dx.doi.org/10.1007/s11263-005-3219-7
18. Ma, W., Morel, J.M., Osher, S., Chien, A.: An l1-based variational model for retinex theory and its application to medical images. In: CVPR, pp. 153–160. IEEE (2011). URL http://dx.doi.org/10.1137/100806588
19. Ma, W., Osher, S.: A tv bregman iterative model of retinex theory. Inverse Problems and Imaging **6**(4), 697–708 (2012). URL http://dx.doi.org/10.3934/ipi.2012.6.697
20. Marini, D., Rizzi, A.: A computational approach to color adaptation effects. Image and Vision Computing **18**(13), 1005–1014 (2000). URL http://dx.doi.org/10.1016/s0262-8856(00)00037-8
21. Morel, J., Petro, A., Sbert, C.: A PDE formalization of retinex theory. Image Processing, IEEE Transactions on **19**(11), 2825–2837 (2010). DOI 10.1109/TIP.2010.2049239. URL http://dx.doi.org/10.1109/tip.2010.2049239
22. Ng, M.K., Wang, W.: A total variation model for retinex. SIAM J. Img. Sci. **4**(1), 345–365 (2011). DOI 10.1137/100806588. URL http://dx.doi.org/10.1137/100806588
23. Papafitsoros, K., Schönlieb, C.: A combined first and second order variational approach for image reconstruction. Journal of Mathematical Imaging and Vision **48**(2), 308–338 (2014). DOI 10.1007/s10851-013-0445-4. URL http://dx.doi.org/10.1007/s10851-013-0445-4
24. Rudin, L.I., Osher, S., Fatemi, E.: Nonlinear total variation based noise removal algorithms. Physica D: Nonlinear Phenomena **60**(1), 259–268 (1992). URL http://dx.doi.org/10.1016/0167-2789(92)90242-f
25. Setzer, S., Steidl, G.: Variational methods with higher order derivatives in image processing. In: N. Press (ed.) Approximation XII, pp. 360–386. Brentwood (2008)
26. Setzer, S., Steidl, G., Teuber, T.: Infimal convolution regularizations with discrete l1-type functionals. Comm. Math. Sci **9**(3), 797–872 (2011). URL http://dx.doi.org/10.4310/cms.2011.v9.n3.a7
27. Tai, X.C., Hahn, J., Chung, G.J.: A fast algorithm for euler's elastica model using augmented lagrangian method. SIAM Journal on Imaging Sciences **4**(1), 313–344 (2011). URL http://dx.doi.org/10.1137/100803730
28. Yin, W., Goldfarb, D., Osher, S.: The Total Variation Regularized L^1 Model for Multiscale Decomposition. Multiscale Modeling and Simulation **6** (2007). DOI 10.1137/060663027. URL http://dx.doi.org/10.1137/060663027
29. Zhang, X., Burger, M., Osher, S.: A unified primal-dual algorithm framework based on Bregman iteration. Journal of Scientific Computing **46**(1), 20–46 (2011). URL http://dx.doi.org/10.1137/09076934X
30. Zosso, D., Tran, G., Osher, S.: A unifying retinex model based on non-local differential operators. In: IS&T/SPIE Electronic Imaging, pp. 865,702–865,702. International Society for Optics and Photonics (2013). URL http://dx.doi.org/10.1117/12.2008839